

Article

Theoretical Study of Hydrogen Production from Ammonia Borane Catalyzed by Metal and Non-Metal Diatom-Doped Cobalt Phosphide

Dong-Heng Li, Qiao-Mei Li, Shuang-Ling Qi, Hai-Chuan Qin, Xiao-Qin Liang and Laicai Li *

College of Chemistry and Material Science, Sichuan Normal University, Chengdu 610068, China

* Correspondence: lilcmail@163.com

Abstract: The decomposition of ammonia borane (NH_3BH_3) to produce hydrogen has developed a promising technology to alleviate the energy crisis. In this paper, metal and non-metal diatom-doped CoP as catalyst was applied to study hydrogen evolution from NH_3BH_3 by density functional theory (DFT) calculations. Herein, five catalysts were investigated in detail: pristine CoP, Ni- and N-doped CoP ($\text{CoP}_{\text{Ni-N}}$), Ga- and N-doped CoP ($\text{CoP}_{\text{Ga-N}}$), Ni- and S-doped CoP ($\text{CoP}_{\text{Ni-S}}$), and Zn- and S-doped CoP ($\text{CoP}_{\text{Zn-S}}$). Firstly, the stable adsorption structure and adsorption energy of NH_3BH_3 on each catalytic slab were obtained. Additionally, the charge density differences (CDD) between NH_3BH_3 and the five different catalysts were calculated, which revealed the interaction between the NH_3BH_3 and the catalytic slab. Then, four different reaction pathways were designed for the five catalysts to discuss the catalytic mechanism of hydrogen evolution. By calculating the activation energies of the control steps of the four reaction pathways, the optimal reaction pathways of each catalyst were found. For the five catalysts, the optimal reaction pathways and activation energies are different from each other. Compared with undoped CoP, it can be seen that $\text{CoP}_{\text{Ga-N}}$, $\text{CoP}_{\text{Ni-S}}$, and $\text{CoP}_{\text{Zn-S}}$ can better contribute hydrogen evolution from NH_3BH_3 . Finally, the band structures and density of states of the five catalysts were obtained, which manifests that $\text{CoP}_{\text{Ga-N}}$, $\text{CoP}_{\text{Ni-S}}$, and $\text{CoP}_{\text{Zn-S}}$ have high-achieving catalytic activity and further verifies our conclusions. These results can provide theoretical references for the future study of highly active CoP catalytic materials.

Keywords: ammonia borane; hydrogen evolution reaction; CoP; diatom-doped; density functional theory



Citation: Li, D.-H.; Li, Q.-M.; Qi, S.-L.; Qin, H.-C.; Liang, X.-Q.; Li, L. Theoretical Study of Hydrogen Production from Ammonia Borane Catalyzed by Metal and Non-Metal Diatom-Doped Cobalt Phosphide. *Molecules* **2022**, *27*, 8206. <https://doi.org/10.3390/molecules27238206>

Academic Editor: Felipe Fantuzzi

Received: 29 October 2022

Accepted: 21 November 2022

Published: 24 November 2022

Publisher's Note: MDPI stays neutral with regard to jurisdictional claims in published maps and institutional affiliations.



Copyright: © 2022 by the authors. Licensee MDPI, Basel, Switzerland. This article is an open access article distributed under the terms and conditions of the Creative Commons Attribution (CC BY) license (<https://creativecommons.org/licenses/by/4.0/>).

1. Introduction

The energy crisis and environmental pollution are two major problems humans are faced with in society today. To deal with these severe problems, taking advantage of renewable energy to replace fossil energy is an important strategy for the international community.

As a renewable energy source, hydrogen energy is light in weight, high in heat, non-toxic, harmless, excellent in thermal conductivity, clean, and pollution-free, which makes it a representative of green energy [1–4]. To date, there are many common industrial hydrogen production methods [5–8], such as the methods of NH_3BH_3 decomposition, water cracking, water and ethanol mixture pulse discharge, etc. However, how to release hydrogen safely and efficiently remains the main obstacle to the spread of hydrogen energy. NH_3BH_3 is considered as one of the most ideal hydrogen storage materials because of its non-toxic, easy storage and transportation and reversible dehydrogenation reaction [9–12]. Catalytic decomposition of NH_3BH_3 is accepted as a promising method for hydrogen production. Although traditional catalysts such as platinum-based or rhodium-based noble metal catalysts have high activity for NH_3BH_3 decomposition, their application is limited due to high cost and short time [13–15]. Therefore, there is an upsurge in research to look for non-noble metal catalysts with high catalytic activity and service life [16–19]. At present,

quantities of composite materials with high catalytic activity and high stability which can catalyze the evolution of hydrogen from ammonia borane have been synthesized [20–24].

Cobalt phosphide (CoP) has become a typical representative of inexpensive transition metal phosphides due to its advantages of low production cost, good stability, and catalytic activity [25–27]. CoP materials include CoP nanowire arrays [28–30], non-metallic-doped CoP materials [31,32], metal-doped CoP materials, etc. [33,34]. Various doped catalytic materials based on cobalt phosphide have been widely studied as excellent catalysts for NH_3BH_3 decomposition to produce hydrogen [35–37], such as non-noble metal cobalt phosphide nanometer materials supported by layered porous carbon (CoPNPs), which were synthesized by step-by-step calcination and phosphating, using a cobalt-based organic framework (CO-MOF-74) as template [38], carbon-point-constrained CoP-CoO nanostructured materials with strong interfacial synergies, which trigger the strong hydrogen evolution performance of NH_3BH_3 [39], nickel-loaded cobalt phosphide (Ni@CoP) materials, etc. [40,41]. These CoP-based modified catalysts improve the hydrogen evolution performance of NH_3BH_3 . It was found that different types of doping have an important effect on the catalytic activity of the materials [42,43]. For example, silver and nitrogen diatom-doped zinc oxide has become a salient way to obtain high quality P-type zinc oxide [44]. The dehydrogenation of NH_3BH_3 catalyzed by Co and Cu diatom-doped magnesium oxide is better than that of Co- and Cu-doped magnesium oxide alone [45]. The catalytic performance and efficiency of O and Mo diatom-doped cobalt phosphide lamellar nanomaterials as catalysts for water cracking has been significantly improved [46].

In view of CoP as an excellent catalyst for the dehydrogenation of NH_3BH_3 and the significant improvement of catalyst performance by diatom-doped metal and non-metal co-doped CoP as a catalyst for hydrogen production from NH_3BH_3 was studied in this paper, and the mechanism of its catalytic dehydrogenation is discussed. At the same time, the catalytic activity of different doped catalysts was studied. The study of the physical properties of doped CoP variants is expected to explain the correlation between the physical properties of the catalysts and the catalytic activity of NH_3BH_3 dehydrogenation, which provides some theoretical references for the optimization and design of the catalysts for hydrogen production from NH_3BH_3 .

2. Calculation Methods

In this study, all the structure optimization, band structures, and density of states (DOS) were calculated using Dmol3 in the Material Studio 8.0 program developed by Accelrys, Inc. The generalized gradient approximation Perdew–Burke–Ernzerhof (PBE) exchange–correlation functional was adopted and the nuclear electron was described by effective core potential (ECP) [47]. To expand the electronic wave function, the double numerical plus polarization (DNP) basis set was used [48]. A $2 \times 2 \times 1$ k-points was sampled using the Monkhorst–Pack method. On this basis, the energy convergence criterion of the self-consistent iterative process was set to 2×10^{-5} Ha, the force convergence accuracy was set to 0.004 Ha/Å, and the maximum displacement was set to 0.005 Å. Meanwhile, The LST/QST method was used to search for reaction transition states whose structures were further confirmed by frequency analysis [49].

A 2×3 CoP (101) slab model with six-layer-atom was built to represent CoP catalysts, which was consistent with that of Deniel et al. [50] and Cao et al. [51,52]. This model contained 72 Co and 72 P atoms. In order to prevent the interactions between periodic images of the slabs, a 15 Å vacuum layer is added in Z direction. In doped CoP, one of the P atoms on pristine CoP (101) surface were replaced by non-metallic N or S atom, and one of the Co atoms on the pristine CoP (101) surface was replaced by Ni, Ga, or Zn atoms, respectively, as shown in Figure 1. Then, metal and non-metal diatom-doped CoP catalyst models were obtained. Herein, we focus on four different types of doped CoP: Ni and N diatom-doped CoP, as denoted $\text{CoP}_{\text{Ni-N}}$; Ga and N diatom-doped CoP, denoted $\text{CoP}_{\text{Ga-N}}$; Ni and S diatom-doped CoP, denoted $\text{CoP}_{\text{Ni-S}}$; and Zn and S diatom-doped CoP, denoted $\text{CoP}_{\text{Zn-S}}$.

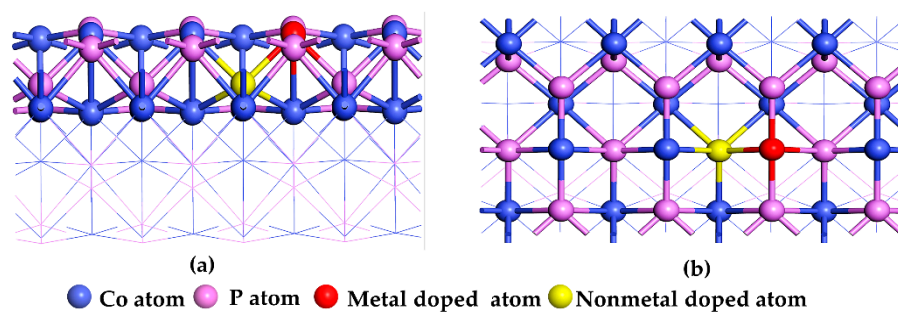


Figure 1. Front view (a) and top view (b) of metal- and non-metal-doped CoP catalyst.

3. Results and Discussions

3.1. Adsorption of NH_3BH_3 on the Surface of CoP and Its Doped Catalysts

The stable adsorption structure of NH_3BH_3 on CoP(101) slabs was obtained by optimizing the model of CoP, as shown in Figure 2. In the optimized adsorption configuration, the H(1) atom on the NH_3BH_3 was adsorbed on the Co(3) atom on the CoP(101) surface, and the distance between the H(1) atom and the Co(3) atom was shortened from 1.79 Å to 1.65 Å. However, the bond length of B-H(1) in NH_3BH_3 increased from 1.26 Å to 1.28 Å. The electron density map of the adsorption configuration of NH_3BH_3 on CoP(101) surface is also shown in Figure 2. It can be seen from Figure 2 that the overlap of electron cloud occurs between H(1) atom of NH_3BH_3 and Co(3) atom of CoP(101) surface, indicating that electron interaction occurs between the H(1) atom of NH_3BH_3 and Co(3) atom on the CoP(101) surface. In the process of adsorption, a part of the energy is released due to the reduction of molecular motion velocity, and this part of the energy is called adsorption energy (E_{ads}), which can be calculated as:

$$E_{\text{ads}} = -(E_{\text{total}} - E_{\text{slab}} - E_{\text{AB}}) \quad (1)$$

In this formula, E_{total} , E_{slab} , and E_{AB} are potential energies of AB adsorbed on the slab model, the slab model, and AB molecule. The adsorption process of NH_3BH_3 on CoP (101) surface is an activation process, and its adsorption energy is -1.19 eV. The other stable adsorption structures of NH_3BH_3 adsorbed on the surface of four different kinds of diatom-doped CoP catalysts ($\text{CoP}_{\text{Ni-N}}$, $\text{CoP}_{\text{Ga-N}}$, $\text{CoP}_{\text{Ni-S}}$, and $\text{CoP}_{\text{Zn-S}}$) are shown in Figure S1. The electron density maps of the adsorption structure are also shown in Figure S1. The adsorption energies of NH_3BH_3 on the four types of doped catalysts are -1.22 ($\text{CoP}_{\text{Ni-N}}$), -1.29 ($\text{CoP}_{\text{Ga-N}}$), -1.21 ($\text{CoP}_{\text{Ni-S}}$), and -1.25 eV ($\text{CoP}_{\text{Zn-S}}$), which indicates that NH_3BH_3 can be stably adsorbed on the surface of the four kinds of doped catalysts, and the adsorption process of NH_3BH_3 on the surface of the four kinds of diatom-doped catalysts is also an activation process.

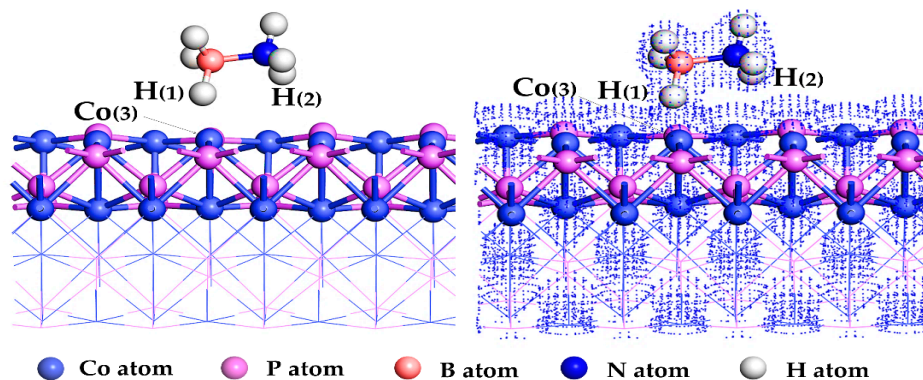


Figure 2. The left shows its adsorption configuration and the right shows the electron density diagram of the adsorption configuration of ammonia borane on the CoP(101) plane.

3.2. Hydrogen Evolution Mechanism of NH_3BH_3 on the Surface of the Catalyst

According to our investigation, there are four potential pathways available for the hydrogen evolution reaction of NH_3BH_3 on the catalyst surfaces, as shown in Figure 3.

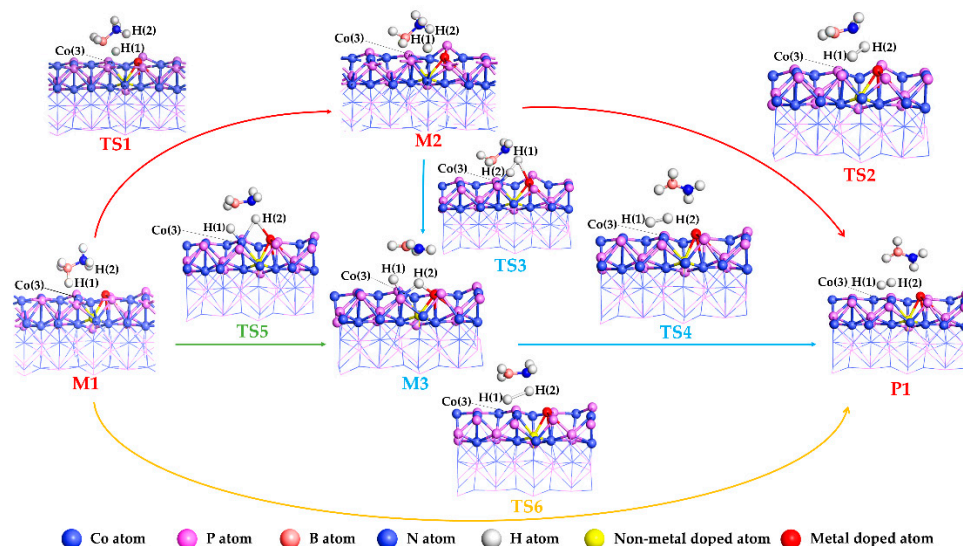


Figure 3. Mechanism of hydrogen evolution reaction of NH_3BH_3 .

Firstly, NH_3BH_3 is adsorbed on the surface of the catalyst to form a stable adsorption reactant denoted as M1 . Then, NH_3BH_3 is dehydrogenated through four different reaction pathways to obtain the product P1 . In the reaction pathway I, the reactant M1 generates the intermediate M2 via the transition state TS1 , and then M2 through the transition state TS2 generates the product P1 . In this process, one of the B-H bonds of the NH_3BH_3 in M1 is broken to become the intermediate M2 via the transition state TS1 . Afterwards, another H atom leaves the N atom of the NH_3BH_2 intermediate, forming bond with the previously generated H atom, generating the final product H_2 and finally completing the hydrogen evolution reaction. In reaction pathway II, the first step of reactant M1 to intermediate M2 is the same as pathway I. After that, one of the N-H bonds of the NH_3BH_3 in M2 is broken to form the intermediate M3 via the transition state TS3 . The configuration of intermediate M3 is that two H atoms are independently adsorbed on the surface of the catalyst. Finally, the two H atoms adsorbed on the surface of the catalyst are combined together to form the final product P1 via transition state TS4 . In the reaction pathway III, the first step is the reactant M1 generates the intermediate M3 via the transition state TS5 , in which, different from reaction pathway II, the N-H and B-H of NH_3BH_3 are broken simultaneously. The following step is that M3 generates the final product P1 via transition state TS4 , which is the same as path II. In reaction pathway IV, the M1 directly generates the H_2 via transition state TS6 .

The structural changes involved in the process of NH_3BH_3 dehydrogenation catalyzed by the five catalysts are shown in Figure 4 ($\text{CoP}_{\text{Zn-S}}$), Supplementary Materials Figure S2 (CoP), Figure S3 ($\text{CoP}_{\text{Ni-N}}$), Figure S4 ($\text{CoP}_{\text{Ga-N}}$), and Figure S5 ($\text{CoP}_{\text{Ni-S}}$). Since each reaction pathway is similar for different catalysts, herein only $\text{CoP}_{\text{Zn-S}}$ is discussed. The relevant structural parameters of the hydrogen evolution reaction catalyzed by $\text{CoP}_{\text{Zn-S}}$ are listed in Table 1, and the relative energies and activation energies in each step are listed in Table 2 and as shown in Figure 4.

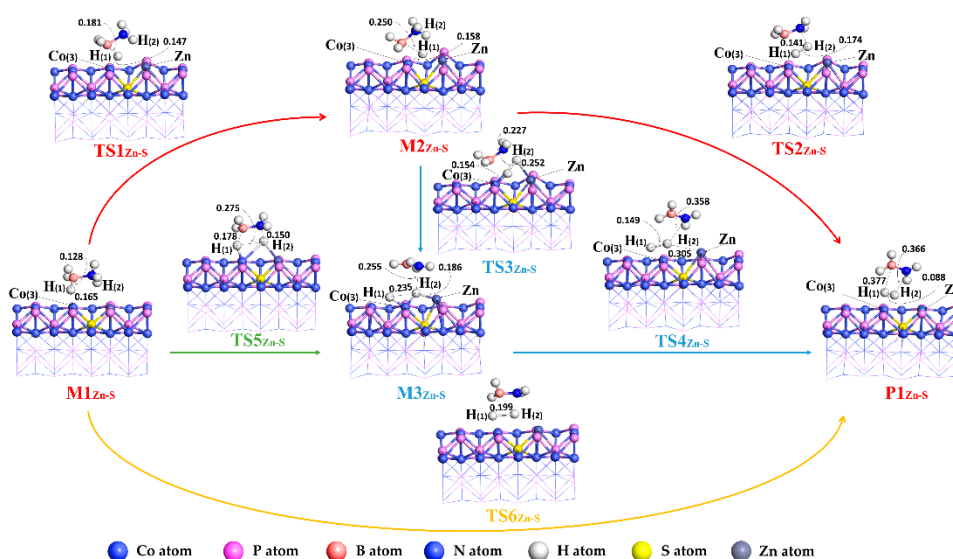


Figure 4. General flowchart of NH_3BH_3 hydrogen production reaction on $\text{CoP}_{\text{Zn-N}}$ (101) surface.

For reaction path I, NH_3BH_3 is adsorbed on the catalyst surface to form $\text{M1}_{\text{Zn-S}}$, and the adsorption site of NH_3BH_3 is above the Co(3) atom on the $\text{CoP}_{\text{Zn-S}}$ surface. Then in $\text{M1}_{\text{Zn-S}}$, the B-H(1) bond is broken, and the H(1) atom escapes from NH_3BH_3 and migrates between the Co(3) and Zn atoms on the surface of $\text{CoP}_{\text{Zn-S}}$, forming intermediate $\text{M2}_{\text{Zn-S}}$ via transition state $\text{TS1}_{\text{Zn-S}}$ with activation energy of 22.71 kcal/mol. In this process, the distance between the B atom and H(1) atom increases from 1.28 Å to 1.81 Å and finally to 2.50 Å from $\text{M1}_{\text{Zn-S}}$ to $\text{TS1}_{\text{Zn-S}}$, forming $\text{M2}_{\text{Zn-S}}$. The distance between H(1) and Co(3) is shortened from 1.65 Å in $\text{M1}_{\text{Zn-S}}$ to 1.47 Å in $\text{TS1}_{\text{Zn-S}}$ and then to 1.58 Å in $\text{M2}_{\text{Zn-S}}$. In the intermediate $\text{M2}_{\text{Zn-S}}$, the H(1) atom on the surface of the catalyst and the H(2) atom on the N atom of NH_3BH_3 converge to form H_2 via transition state $\text{TS2}_{\text{Zn-S}}$. The activation energy of $\text{TS2}_{\text{Zn-S}}$ is 39.56 kcal/mol. The distance between the H(1) atom and Co(3) changes from 1.58 Å to 1.52 Å, and the distance between the H(1) atom and H(2) decreases from 2.41 Å to 1.72 Å. In the process of $\text{M2}_{\text{Zn-S}} \rightarrow \text{TS2}_{\text{Zn-S}} \rightarrow \text{P1}_{\text{Zn-S}}$, the distance between H(2) and N atoms changes from 1.05 Å to 1.92 Å and finally to 3.66 Å.

For reaction pathway II, firstly, the reactant NH_3BH_3 is adsorbed on the surface of the catalyst to form $\text{M1}_{\text{Zn-S}}$, and the $\text{M1}_{\text{Zn-S}}$, through the transition state $\text{TS1}_{\text{Zn-S}}$, forms the intermediate $\text{M2}_{\text{Zn-S}}$, which is the same as the process of $\text{M1}_{\text{Zn-S}} \rightarrow \text{M2}_{\text{Zn-S}}$ in pathway I. Subsequently, in the intermediate $\text{M2}_{\text{Zn-S}}$, the H(2) atom on the N atom of NH_3BH_3 is gradually detached from the NH_3BH_3 and adsorbed between the Co(3) and Zn on the CoP (101) surface of the catalyst. With the movement of the H(2) atom, the H(1) atom is adsorbed to the upper left of the Co(3) atom to form the intermediate $\text{M3}_{\text{Zn-S}}$, which is the transition state $\text{TS3}_{\text{Zn-S}}$ with an activation energy of 42.04 kcal/mol. In this process, the distance between the H(2) atom and the N atom of NH_3BH_3 increases from 1.05 Å to 1.51 Å and finally to 2.55 Å in $\text{M3}_{\text{Zn-S}}$. The distance between the H(1) and Co(3) atoms varies from 1.58 Å for $\text{M2}_{\text{Zn-S}}$ to 1.54 Å for $\text{TS3}_{\text{Zn-S}}$ and finally to 1.65 Å for $\text{M3}_{\text{Zn-S}}$. The distances between H(2) and Co(3), H(2), and Zn vary from 3.31 Å and 2.96 Å in $\text{M2}_{\text{Zn-S}}$ to 3.15 Å and 2.52 Å in $\text{TS3}_{\text{Zn-S}}$ and finally to 1.59 Å and 3.05 Å in $\text{M3}_{\text{Zn-S}}$. In the intermediate $\text{M3}_{\text{Zn-S}}$, the two H atoms adsorbed on the surface of the catalyst are close to each other via the transition state $\text{TS4}_{\text{Zn-S}}$ to form product P1. The activation energy of the transition state $\text{TS4}_{\text{Zn-S}}$ is 9.73 kcal/mol.

For reaction path III, the reactant NH_3BH_3 is first adsorbed on the catalyst surface to form $\text{M1}_{\text{Zn-S}}$. Then, the H(1) and H(2) atoms, respectively cleaved from the B and N atoms of NH_3BH_3 , were adsorbed on the surface of the catalyst above the Zn atom of Co(3) atom to form the intermediate $\text{M3}_{\text{Zn-S}}$ through the transition state $\text{TS5}_{\text{Zn-S}}$ with an activation energy of 28.80 kcal/mol. In this process, the distance between the B atom and

H(1) atom increases from 1.28 Å to 0.178 Å, and the distance between the H(2) atom and N atom increases from 1.03 Å to 1.50 Å. The intermediate M3_{Zn-S} through the transition state TS4_{Zn-S} forms the product P1_{Zn-S}, which is consistent with the process of M3_{Zn-S}→P1_{Zn-S} in path II.

For reaction path IV, in M1_{Zn-S}, the H atom on the B atom of NH₃BH₃ and the H atom on the N atom of NH₃BH₃ directly generated the H₂ via the transition state TS6_{Zn-S} with the activation energy of 22.15 kcal/mol, in which the distance between the H(1) and H(2) atoms decreases from 2.53 Å to 1.99 Å in TS6_{Zn-S}.

Table 1. The bond length (Å) parameters of reaction sites in CoP_{Zn-S}-catalyzed NH₃BH₃ hydrogen evolution process. (Å).

Pathway	B-H(1)	Co(3)-H(1)	N-H(2)	Co(3)-H(2)	Zn-H(2)	H(1)-H(2)	
I	M1 _{Zn-S}	1.28	1.65	1.03	–	–	2.53
	TS1 _{Zn-S}	1.81	1.47	1.02	–	–	2.19
	M2 _{Zn-S}	2.50	1.58	1.05	–	–	2.41
	TS2 _{Zn-S}	2.61	1.52	1.92	–	–	1.72
	P1 _{Zn-S}	3.77	1.62	3.66	–	–	0.88
II	M1 _{Zn-S}	–	1.65	1.03	3.45	3.03	2.53
	TS1 _{Zn-S}	–	1.47	1.02	3.29	2.66	2.19
	M2 _{Zn-S}	–	1.58	1.05	3.31	2.96	2.41
	TS3 _{Zn-S}	–	1.54	1.51	3.15	2.52	2.27
	M3 _{Zn-S}	–	1.65	2.55	1.60	1.86	2.35
	TS4 _{Zn-S}	–	1.63	3.58	1.59	3.05	1.49
	P1 _{Zn-S}	–	1.62	3.66	1.61	3.86	0.09
III	M1 _{Zn-S}	1.28	1.65	1.03	3.45	3.03	2.53
	TS5 _{Zn-S}	1.78	1.62	1.50	2.78	2.37	2.75
	M3 _{Zn-S}	3.33	1.63	2.55	1.59	3.05	2.35
	TS4 _{Zn-S}	3.83	1.63	3.58	1.59	3.05	1.49
	P1 _{Zn-S}	3.77	1.62	3.66	1.61	3.86	0.88
IV	M1 _{Zn-S}	1.28	–	1.03	–	–	2.53
	TS6 _{Zn-S}	2.30	–	1.91	–	–	1.99
	P1 _{Zn-S}	3.77	–	3.66	–	–	0.88

The reaction mechanisms of pristine CoP, CoP_{Ni-N}, CoP_{Ga-N}, or CoP_{Ni-S} catalyzed NH₃BH₃ are similar to the CoP_{Zn-S} catalyst. The details of the configuration changes and configuration parameters of the reaction process are shown in Supplementary Materials Figure S2 (CoP), Figure S3 (CoP_{Ni-N}), Figure S4 (CoP_{Ga-N}), and Figure S5 (CoP_{Ni-S}). The changes in structural parameters are shown in Supplementary Materials Table S1 (CoP), Table S2 (CoP_{Ni-N}), Table S3 (CoP_{Ga-N}), and Table S4 (CoP_{Ni-S}). The results from the configuration changes in the reaction process of Figures S2 and S3–S5, can also indicate that the reaction mechanism of CoP and the other diatom-doped CoP catalysts has small differences.

The conclusion can be draw from Table 2 that in the reaction of NH₃BH₃ dehydrogenation catalyzed by CoP_{Zn-S}, the control steps of each reaction pathway are different, (CoP, CoP_{Ni-N}, CoP_{Ga-N}, CoP_{Ni-S}, as shown in Tables S5–S8) which are M2_{Zn-S}→TS2_{Zn-S} (pathway I), M2_{Zn-S}→TS3_{Zn-S} (pathway II), M1_{Zn-S}→TS5_{Zn-S} (pathway III), and M1_{Zn-S}→TS6_{Zn-S} (pathway IV), respectively. The energy barrier values of each control step are 39.56 kcal/mol (pathway I), 42.04 kcal/mol (pathway II), 28.08 (pathway III) kcal/mol and 22.15 kcal/mol (pathway IV), respectively. According to the comparison of activation energy of each reaction path control step, the optimal pathway of the NH₃BH₃ dehydrogenation reaction is reaction pathway IV, and the energy barrier of the control step is 22.15 kcal/mol.

Table 2. The each position energies (E), relative energies (E_{rel}) and activation energies (E_a) of ammoborane reaction catalyzed by CoP_{Zn-S} .

Pathway	Compound	E_{rel}	E_a
		kcal/mol	kcal/mol
pathway I	$M1_{Zn-S}$	0.00	
	$TS1_{Zn-S}$	22.71	22.71
	$M2_{Zn-S}$	−4.83	
	$TS2_{Zn-S}$	37.21	39.56
	$P1_{Zn-S}$	−29.93	
pathway II	$M1_{Zn-S}$	0.00	
	$TS1_{Zn-S}$	22.71	22.71
	$M2_{Zn-S}$	−4.83	
	$TS3_{Zn-S}$	37.21	42.04
	$M3_{Zn-S}$	−29.93	
	$TS4_{Zn-S}$	−20.20	9.73
pathway III	$P1_{Zn-S}$	−26.62	
	$M1_{Zn-S}$	0.00	
	$TS5_{Zn-S}$	28.80	28.80
	$M3_{Zn-S}$	−29.93	
	$TS4_{Zn-S}$	−20.20	9.73
pathway IV	$P1_{Zn-S}$	−26.62	
	$M1_{Zn-S}$	0.00	
	$TS6_{Zn-S}$	22.15	22.15

Considering the energy changes in the five catalysts, the activation energies of CoP , CoP_{Ni-N} , CoP_{Ga-N} , CoP_{Ni-S} , and CoP_{Zn-S} catalyzing the decomposition of NH_3BH_3 to hydrogen at each step are listed in Table 3. In CoP -catalyzed NH_3BH_3 dehydrogenation, as shown in Table S5, the activation energy of the optimal control step of the four reaction pathways is 31.35 kcal/mol. The activation energies of CoP_{Ni-N} , CoP_{Ga-N} , and CoP_{Ni-S} are 27.11 kcal/mol, 23.18 kcal/mol, and 20.67 kcal/mol, respectively. The energy level changes of the five catalysts in the reaction process are shown in Figure S6 (CoP), Figure S7 (CoP_{Ni-N}), Figure S8 (CoP_{Ga-N}), Figure S9 (CoP_{Ni-S}), and Figure S10 (CoP_{Zn-S}). By comparing the catalytic activities of CoP , CoP_{Ni-N} , CoP_{Ga-N} , CoP_{Ni-S} , and CoP_{Zn-S} , it is found that the simultaneous doping of metal and non-metal with CoP is beneficial to the improvement of NH_3BH_3 hydrogen evolution activity. A large number of studies on cobalt-phosphide-modified materials can prove that the dopant of N, S, Ni, Zn, and Ga can improve the catalytic performance of CoP , which is consistent with our theoretical calculation results. For instance, Chen et al. [53] reported that Ni-doped CoP could accelerate the process of hydrogen evolution both in acid and alkaline media, showing excellent electrochemical stability and durability. Li et al. [54] found N and Mo co-doped heteroatoms can optimize the morphology and surface structure of CoP . Anjum et al. [55] studied sulfur-doped cobalt phosphide electrocatalysts and concluded that their performance is better than all-noble-metal electrocatalysts in alkaline electrolyzers for overall water splitting. Yang et al. [56] synthesized Zn-doped CoP nanowire arrays for boosting hydrogen generation, and they found the overpotential of Zn-doped CoP was two times lower than undoped CoP . Zhang et al. [57] also reported that Ga dopant could enhance the activity of CoP .

Table 3. The reaction pathway activation energies of five catalysts in pathway I–IV (kcal/mol).

Pathway	Compound	CoP	CoP _{Ni-N}	CoP _{Ga-N}	CoP _{Ni-S}	CoP _{Zn-S}
pathway I	TS1	21.88	29.15	22.48	20.67	22.71
	TS2	51.65	44.87	65.63	45.16	39.56
pathway II	TS1	21.88	29.15	22.48	20.67	22.71
	TS3	31.35	35.81	23.18	19.14	42.04
	TS4	0.57	5.27	6.67	7.40	9.73
pathway III	TS5	36.68	33.45	47.29	47.94	28.80
	TS4	0.57	5.27	6.67	7.40	9.73
pathway IV	TS6	52.02	27.11	44.19	48.48	22.15

3.3. Performance Calculation of Catalysts

The stable catalyst models of CoP, CoP_{Ni-N}, CoP_{Ga-N}, CoP_{Ni-S}, and CoP_{Zn-S} were optimized and obtained. The band structure and density of states (DOS) of the stable catalyst were calculated, as shown in Figure S11. The diagram of band structure is marked by 1 on the left, and the map of density of states is marked by 2 on the right, in which a1, b1, c1, d, and e1 represent the band structure diagram of CoP, CoP_{Ni-N}, CoP_{Ga-N}, CoP_{Ni-S}, and CoP_{Zn-S}, respectively. Meanwhile, a2, b2, c2, d2, and e2 represent the map of density of states of CoP, CoP_{Ni-N}, CoP_{Ga-N}, CoP_{Ni-S}, and CoP_{Zn-S}. The red dashed line in the figure represents the Fermi level.

The DOS map, which refers to the number of states in a unit frequency interval, is used to characterize the distribution of electron cloud density near the Fermi level. The Fermi level is a parameter used to measure the catalytic activity, and its value is the average of the sum of the highest energy occupied orbital and the lowest energy occupied orbital. The greater the density of the electron cloud near the Fermi level, the stronger the catalytic activity of the material. We calculated the total DOS of the five catalysts at the Fermi level as follows: 37.4 (CoP), 41.9 (CoP_{Ni-N}), 42.8 (CoP_{Ga-N}), 43.8 (CoP_{Ni-S}), and 42.1 (CoP_{Zn-S}), indicating that the electron cloud density near the Fermi level of CoP_{Ni-N}, CoP_{Ga-N}, CoP_{Ni-S}, and CoP_{Zn-S} increases compared with pristine CoP. This may be the reason why CoP_{Ni-N}, CoP_{Ga-N}, CoP_{Ni-S}, and CoP_{Zn-S} are able to improve the activity of NH₃BH₃ hydrogen evolution. Sun et al. reported similar studies on polysulfur confinement and the electrochemical kinetics of amorphous cobalt phosphide-enhanced lithium-sulfur batteries [58].

In the end, to research the effect of interfacial adsorption on catalytic activity for the five doped catalysts, the charge density difference (CDD) between NH₃BH₃ and the five different catalysts were calculated. CDD is one of the important methods to study electronic structure. The electron flow direction after the interaction of each segment can be intuitively obtained, or the change of electron density during the formation of atoms into molecules, and the nature of chemical bonds can be explored. As shown in Figure 5, blue is the electron accumulation, while red represents the electron depletion. From Figure 5, we can realize the charge transfer characteristics of NH₃BH₃ and the five catalytic adsorption processes. Compared with undoped CoP, the electronic interaction between doped catalysts and NH₃BH₃ is enhanced, which indicates the strong electronic interaction between the catalyst and NH₃BH₃, determining the catalytic activity in the adsorption process.

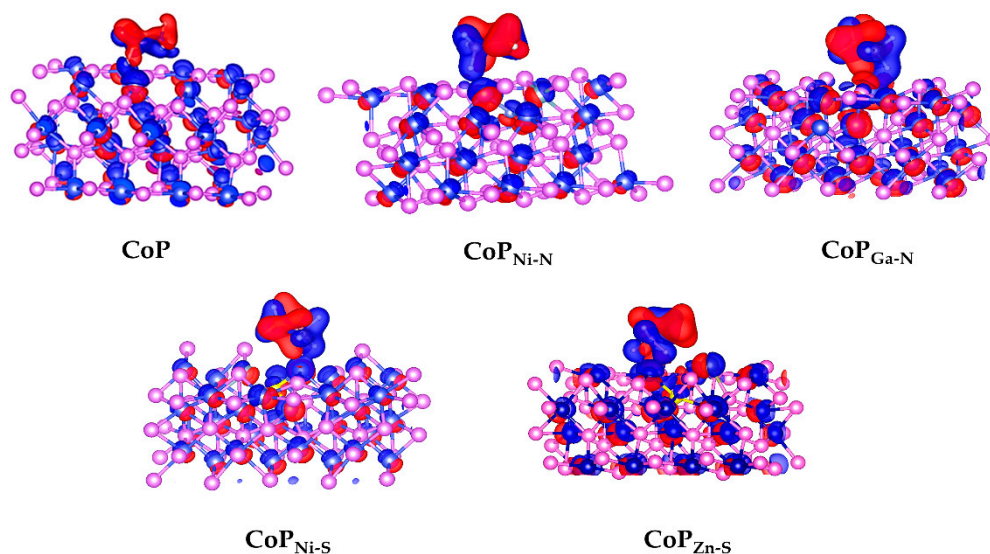


Figure 5. CDDs maps of CoP, CoP_{Ni-N}, CoP_{Ga-N}, CoP_{Ni-S}, and CoP_{Zn-S} catalyzed NH₃BH₃.

4. Conclusions

In this paper, metal and non-metal diatom-doped CoP as catalyst was applied to study hydrogen evolution from NH₃BH₃ by DFT calculations. The doped catalysts involved in CoP_{Ni-N}, CoP_{Ga-N}, CoP_{Ni-S}, and CoP_{Zn-S} were formed by replacing Co atoms with Ni, Ga, or Zn, and P atoms with S or N on the surface of the CoP(101), respectively. First of all, the adsorption process of NH₃BH₃ on each catalyst was explored, and the adsorption energy and electron density maps were obtained. From the values of adsorption energies and electron density maps, the conclusion can be drawn that each doped type of catalyst has a strong adsorption effect on NH₃BH₃, which is activated on the surface of the catalyst. Then, we further studied the reaction mechanism of the decomposition of NH₃BH₃ into H₂ and NH₂BH₂ catalyzed by five catalysts (CoP, CoP_{Ni-N}, CoP_{Ga-N}, CoP_{Ni-S}, and CoP_{Zn-S}). In this investigation, four pathways were designed, and the best reaction pathways for each catalyst were found. By analyzing the activation energy of the control step, it can be seen clearly that the energy barrier values of the control step for the five catalysts are $E_a(\text{CoP}) > E_a(\text{CoP}_{\text{Ni-N}}) > E_a(\text{CoP}_{\text{Ga-N}}) > E_a(\text{CoP}_{\text{Zn-S}}) > E_a(\text{CoP}_{\text{Ni-S}})$. According to the energy barrier results, the activity of the five catalysts should be $\text{CoP}_{\text{Ni-S}} > \text{CoP}_{\text{Zn-S}} > \text{CoP}_{\text{Ga-N}} > \text{CoP}_{\text{Ni-N}}$. Finally, the structural performance of the catalyst was investigated, and the band structure and DOS of the CoP_{Ni-N}, CoP_{Ga-N}, CoP_{Ni-S}, and CoP_{Zn-S} catalysts were calculated. The total DOS of the five catalysts at the Fermi level are 37.4 (CoP), 41.1 (CoP_{Ni-N}), 42.8 (CoP_{Ga-N}), 43.8 (CoP_{Ni-S}), and 42.1 (CoP_{Zn-S}). The study results we obtained have revealed the relationship between the physical properties of doped CoP materials and their catalytic activities, which provides theoretical support for a large number of high-activity cobalt phosphide materials doped with non-metals (N, S) and metals (Ni, Ga, Zn) and references for the future study of highly active CoP catalytic materials.

Supplementary Materials: The following supporting information can be downloaded at: <https://www.mdpi.com/article/10.3390/molecules27238206/s1>, Figure S1: Stable structures and electron density maps of NH₃BH₃ absorbed on the surface of four different kinds of diatom-doped CoP catalysts (CoP_{Ni-N}, CoP_{Ga-N}, CoP_{Ni-S} and CoP_{Zn-S}); Figure S2: General flow chart of NH₃BH₃ hydrogen production reaction on CoP (101) surface; Figure S3: General flow chart of NH₃BH₃ hydrogen production reaction on CoP_{Ni-N} (101) surface; Figure S4: General flow chart of NH₃BH₃ hydrogen production reaction on CoP_{Ga-N} (101) surface; Figure S5: General flow chart of NH₃BH₃ hydrogen production reaction on CoP_{Ga-N} (101) surface; Figure S6: The energy profiles of NH₃BH₃ dehydrogenation reaction catalyzed by CoP; Figure S7: The energy profiles of NH₃BH₃ dehydrogenation reaction catalyzed by CoP_{Ni-N}; Figure S8: The energy profiles of NH₃BH₃ dehydrogenation reaction catalyzed by CoP_{Ga-N}; Figure S9: The energy profiles of NH₃BH₃ dehydrogenation reaction catalyzed

by $\text{CoP}_{\text{Ga-N}}$; Figure S10: The energy profiles of NH_3BH_3 dehydrogenation reaction catalyzed by $\text{CoP}_{\text{Ga-N}}$; Figure S11: Schematic diagram of energy band structure(EBS) and density of states(DOS). (subscript 1 is EBS, subscript 2 is DOS, (a), (b), (c), (d), (e) refer to CoP, $\text{CoP}_{\text{Ni-N}}$, $\text{CoP}_{\text{Ga-N}}$, $\text{CoP}_{\text{Ni-S}}$, $\text{CoP}_{\text{Zn-S}}$ respectively); Table S1: Bond lengths (nm) of various sites in the reaction of NH_3BH_3 catalyzed by CoP; Table S2: Bond lengths (nm) of various sites in the reaction of NH_3BH_3 catalyzed by $\text{CoP}_{\text{Ni-N}}$; Table S3: Bond lengths (nm) of various sites in the reaction of NH_3BH_3 catalyzed by $\text{CoP}_{\text{Ga-N}}$; Table S4: Bond lengths (nm) of various sites in the reaction of NH_3BH_3 catalyzed by $\text{CoP}_{\text{Ni-S}}$; Table S5: The each position energies (E), relative energies (E_{rel}) and activation energies (E_{a}) of ammorbore reaction catalyzed by CoP; Table S6: The each position energies (E), relative energies (E_{rel}) and activation energies (E_{a}) of ammorbore reaction catalyzed by $\text{CoP}_{\text{Ni-N}}$; Table S7: The each position energies (E), relative energies (E_{rel}) and activation energies (E_{a}) of ammorbore reaction catalyzed by $\text{CoP}_{\text{Ga-N}}$; Table S8: The each position energies (E), relative energies (E_{rel}) and activation energies (E_{a}) of ammorbore reaction catalyzed by $\text{CoP}_{\text{Ni-S}}$.

Author Contributions: Conceptualization, D.-H.L., H.-C.Q., Q.-M.L., S.-L.Q., X.-Q.L. and L.L.; methodology, X.-Q.L. and L.L.; validation, D.-H.L. and H.-C.Q.; formal analysis, D.-H.L., Q.-M.L. and S.-L.Q.; resources, H.-C.Q. and L.L.; data curation, D.-H.L. and H.-C.Q.; writing—original draft preparation, H.-C.Q.; writing—review and editing, D.-H.L. All authors have read and agreed to the published version of the manuscript.

Funding: This work has been supported by the High Performance Computing Center of Sichuan Normal University.

Institutional Review Board Statement: Not applicable.

Informed Consent Statement: The authors declare no competing financial interest.

Data Availability Statement: The data presented in this study are available on reasonable request from the corresponding author.

Acknowledgments: This work has been supported by the High Performance Computing Center of Sichuan Normal University. The authors are grateful to College of Chemistry and Material Science, Sichuan Normal University.

Conflicts of Interest: The authors declare no conflict of interest.

References

1. Liu, L.; Sun, Z.; Zhang, L. Progress in Global Gas Hydrate Development and Production as a New Energy Resource. *Acta Geol. Sin.* **2019**, *93*, 731–755. [[CrossRef](#)]
2. Yang, Z. Research on New Energy-saving and Efficient Utilization of Buildings Based on Renewable Energy. *IOP Conf. Ser. Earth Environ. Sci.* **2020**, *514*, 042016. [[CrossRef](#)]
3. Manousiouthakis, V.; Cabezas, H. Editorial Overview: Hydrogen Energy; Sources and Various Issues. *Curr. Opin. Chem. Eng.* **2018**, *21*, i–iii. [[CrossRef](#)]
4. Zhan, T.; Bie, R.; Shen, Q.; Lin, L.; Wu, A.; Dong, P. Application of Electrolysis Water Hydrogen Production in the Field of Renewable Energy Power Generation. *IOP Conf. Ser. Earth Environ. Sci.* **2020**, *598*, 012088. [[CrossRef](#)]
5. Bajus, S.; Agel, F.; Kusche, M.; Ni Bhriaina, N.; Wasserscheid, P. Alkali hydroxide-modified Ru/ $\gamma\text{-Al}_2\text{O}_3$ catalysts for ammonia decomposition. *Appl. Catal. A* **2016**, *510*, 189–195. [[CrossRef](#)]
6. Wang, Y.; Jin, F.; Zeng, X.; Yao, G.; Jing, Z. A novel method for producing hydrogen from water with Fe enhanced by HS—under mild hydrothermal conditions. *Int. J. Hydrogen Energy* **2013**, *38*, 760–768. [[CrossRef](#)]
7. Xin, Y.; Sun, B.; Zhu, X.; Yan, Z.; Zhao, X.; Sun, X.; Takayuki, O. Characteristics and pathways of hydrogen produced by pulsed discharge in ethanol-water mixtures. *Int. J. Hydrogen Energy* **2020**, *45*, 1588–1596. [[CrossRef](#)]
8. Li, X.; Li, Z.; Yang, J. Proposed photosynthesis method for producing hydrogen from dissociated water molecules using incident near-infrared light. *Phys. Rev. Lett.* **2014**, *112*, 018301. [[CrossRef](#)] [[PubMed](#)]
9. Rossin, A.; Peruzzini, M. Ammonia-Borane and Amine-Borane Dehydrogenation Mediated by Complex Metal Hydrides. *Chem. Rev.* **2016**, *116*, 8848–8872. [[CrossRef](#)]
10. Wu, H.; Cheng, Y.J.; Fan, Y.P.; Lu, X.M.; Li, L.X.; Liu, B.Z.; Li, B.J.; Lu, S.Y. Metal-catalyzed hydrolysis of ammonia borane: Mechanism, catalysts, and challenges. *Int. J. Hydrogen Energy* **2020**, *45*, 30325–30340. [[CrossRef](#)]
11. Demirci, U.B. Ammonia borane, a material with exceptional properties for chemical hydrogen storage. *Int. J. Hydrogen Energy* **2017**, *42*, 9978–10013. [[CrossRef](#)]
12. Staubitz, A.; Robertson, A.P.M.; Manners, I. Ammonia-borane and related compounds as dihydrogen sources. *Chem. Rev.* **2010**, *110*, 4079–4124. [[CrossRef](#)] [[PubMed](#)]

13. Mori, K.; Miyawaki, K.; Yamashita, H. Ru and Ru-Ni Nanoparticles on TiO₂ Support as Extremely Active Catalysts for Hydrogen Production from Ammonia-Borane. *ACS Catal.* **2016**, *6*, 3128–3135. [[CrossRef](#)]
14. Blaquiere, N.; Diallo-Garcia, S.; Gorelsky, S.I.; Black, D.A.; Fagnou, K. Ruthenium-catalyzed dehydrogenation of ammonia boranes. *J. Am. Chem. Soc.* **2008**, *130*, 14034–14035. [[CrossRef](#)]
15. Chen, G.Z.; Desinan, S.; Rosei, R.; Rosei, F.; Ma, D.L. Hollow ruthenium nanoparticles with small dimensions derived from Ni@Ru core@shell structure: Synthesis and enhanced catalytic dehydrogenation of ammonia borane. *Chem. Commun.* **2012**, *48*, 8009–8011. [[CrossRef](#)]
16. Huo, J.R.; Fu, L.; Zhao, C.X.; He, C.Z. Hydrogen generation of ammonia borane hydrolysis catalyzed by Fe₂₂@Co₅₈ core-shell structure. *Chin. Chem. Lett.* **2021**, *32*, 2269–2273. [[CrossRef](#)]
17. Zhang, J.P.; Li, J.; Yang, L.J.; Li, R.; Zhang, F.M.; Dong, H. Efficient hydrogen production from ammonia borane hydrolysis catalyzed by TiO₂-supported RuCo catalysts. *Int. J. Hydrogen Energy* **2021**, *46*, 3964–3973. [[CrossRef](#)]
18. Alpaydin, C.Y.; Gulbay, S.K.; Colpan, C.O. A review on the catalysts used for hydrogen production from ammonia borane. *Int. J. Hydrogen Energy* **2020**, *45*, 3414–3434. [[CrossRef](#)]
19. Xu, P.; Lu, W.W.; Zhang, J.J.; Zhang, L. Efficient hydrolysis of ammonia borane for hydrogen evolution catalyzed by plasmonic Ag@Pd core-shell nanocubes. *ACS Sustain. Chem. Eng.* **2020**, *8*, 12366–12377. [[CrossRef](#)]
20. Liao, J.Y.; Feng, Y.F.; Zhang, X.B.; Huang, S.Q.; Liu, M.W.; Liu, Q.B.; Li, H. CuO-Co₃O₄ Composite Nanoplatelets for Hydrolyzing Ammonia Borane. *ACS Appl. Nano Mater.* **2021**, *4*, 7640–7649. [[CrossRef](#)]
21. Feng, Y.F.; Zhang, X.F.; Shao, Y.X.; Chen, X.D.; Wang, H.Z.; Li, J.H.; Wu, M.; Dong, H.F.; Liu, Q.B.; Li, H. Modulating the Acidic Properties of Mesoporous Mo_x-Ni_{0.8}Cu_{0.2}O Nanowires for Enhanced Catalytic Performance toward the Methanolysis of Ammonia Borane for Hydrogen Production. *ACS Appl. Mater. Interfaces* **2022**, *14*, 27979–27993. [[CrossRef](#)] [[PubMed](#)]
22. Liao, J.Y.; Shao, Y.X.; Feng, Y.F.; Zhang, J.; Song, C.X.; Zeng, W.; Tang, J.T.; Dong, H.F.; Liu, Q.B.; Li, H. Interfacial Charge Transfer Induced Dual-active-sites of Heterostructured Cu_{0.8}Ni_{0.2}WO₄ Nanoparticles in Ammonia Borane Methanolysis for Fast Hydrogen Production. *Appl. Catal. B Environ.* **2023**, *320*, 121973. [[CrossRef](#)]
23. Feng, Y.F.; Shao, Y.X.; Chen, X.D.; Zhang, Y.D.; Liu, Q.B.; He, M.Y.; Li, H. Sea-Urchin-like Hollow CuMoO₄-CoMoO₄ Hybrid Microspheres, a Noble-Metal-like Robust Catalyst for the Fast Hydrogen Production from Ammonia Borane. *ACS Appl. Energy Mater.* **2021**, *4*, 633–642. [[CrossRef](#)]
24. Liao, J.Y.; Wu, Y.J.; Shao, Y.X.; Feng, Y.F.; Zhang, X.F.; Zhang, W.L.; Li, J.H.; Wu, M.; Dong, H.F.; Liu, Q.B.; et al. Ammonia Borane Methanolysis for Hydrogen Evolution on Cu₃Mo₂O₉/NiMoO₄ Hollow Microspheres. *Chem. Eng. J.* **2022**, *449*, 137755. [[CrossRef](#)]
25. Liu, Q.; Tian, J.Q.; Cui, W.; Jiang, P.; Cheng, N.Y.; Asiri, A.M.; Sun, X.P. Carbon nanotubes decorated with CoP nanocrystals: A highly active non-noble-metal nanohybrid electrocatalyst for hydrogen evolution. *Angew. Chem. Int. Ed.* **2014**, *53*, 6710–6714. [[CrossRef](#)]
26. Tang, C.; Zhang, R.; Lu, W.B.; He, L.B.; Jiang, X.; Asiri, A.M.; Sun, X.P. Fe-Doped CoP Nanoarray: A Monolithic Multifunctional Catalyst for Highly Efficient Hydrogen Generation. *Adv. Mater.* **2017**, *29*, 1602441. [[CrossRef](#)] [[PubMed](#)]
27. Xu, S.R.; Yu, X.; Liu, X.; Teng, C.L.; Du, Y.S.; Wu, Q. Contrrollable synthesis of peony-like porous Mn-CoP nanorod electrocatalyst for highly efficient hydrogen evolution in acid and alkaline. *J. Colloid Interface Sci.* **2020**, *577*, 379–387. [[CrossRef](#)]
28. Ren, Y.C.; Li, Z.R.; Deng, B.; Ye, C.; Zhang, L.C.; Wang, Y.; Li, T.S.; Liu, Q.; Cui, G.W.; Asiri, A.M.; et al. Superior hydrogen evolution electrocatalysis enabled by CoP nanowire array on graphite felt. *Int. J. Hydrogen Energy* **2022**, *47*, 3580–3586. [[CrossRef](#)]
29. Zhu, D.D.; Wang, L.; Qiao, M.; Liu, J.L. Phosphate ion functionalized CoP nanowire arrays for efficient alkaline hydrogen evolution. *Chem. Commun.* **2020**, *56*, 7159–7162. [[CrossRef](#)]
30. Jing, Y.Q.; Liu, H.L.; Yang, R.J.; Chen, J.; Dai, H.T.; Liu, C.L.; Zhang, X.D. Mesoporous CoP nanowire arrays for hydrogen evolution. *ACS Appl. Nano Mater.* **2019**, *2*, 5922–5930. [[CrossRef](#)]
31. Ma, L.Z.; Guo, J.X. S-doped CoP nanoneedles assembled urchin-like structure for efficient water oxidation. *Mater. Lett.* **2022**, *307*, 131005. [[CrossRef](#)]
32. Liu, Z.; Yu, X.; Xue, H.G.; Feng, L.G. A nitrogen-doped CoP nanoarray over 3D porous Co foam as an efficient bifunctional electrocatalyst for overall water splitting. *J. Mater. Chem. A* **2019**, *7*, 13242–13248. [[CrossRef](#)]
33. Zhang, R.; Tang, C.; Kong, R.M.; Du, G.; Asiri, A.M.; Chen, L.; Sun, X.P. Al-Doped CoP nanoarray: A durable water-splitting electrocatalyst with superhigh activity. *Nanoscale* **2017**, *9*, 4793–4800. [[CrossRef](#)] [[PubMed](#)]
34. Li, X.M.; Li, S.S.; Yoshida, A.; Sirisomboonchai, S.; Tang, K.Y.; Zuo, Z.J.; Hao, X.G.; Abudula, A.; Guan, G.Q. Mn doped CoP nanoparticle clusters: An efficient electrocatalyst for hydrogen evolution reaction. *Catal. Sci. Technol.* **2018**, *8*, 4407–4412. [[CrossRef](#)]
35. Pan, Y.; Sun, K.A.; Lin, Y.; Cao, X.; Cheng, Y.S.; Liu, S.J.; Zeng, L.Y.; Cheong, W.C.; Zhao, D.; Wu, K.L.; et al. Electronic structure and d-band center control engineering over M-doped CoP (M = Ni, Mn, Fe) hollow polyhedron frames for boosting hydrogen production. *Nano Energy* **2019**, *56*, 411–419. [[CrossRef](#)]
36. Wang, X.Q.; Chen, Y.F.; Yu, B.; Wang, Z.G.; Wang, H.Q.; Sun, B.C.; Li, W.X.; Yang, D.X.; Zhang, W.L. Hierarchically Porous W-Doped CoP Nanoflake Arrays as Highly Efficient and Stable Electrocatalyst for pH-Universal Hydrogen Evolution. *Small* **2019**, *15*, 1902613. [[CrossRef](#)]
37. Zhou, Q.W.; Shen, Z.H.; Zhu, C.; Li, J.C.; Ding, Z.Y.; Wang, P.; Pan, F.; Zhang, Z.Y.; Ma, H.X.; Wang, S.Y.; et al. Nitrogen-Doped CoP Electrocatalysts for Coupled Hydrogen Evolution and Sulfur Generation with Low Energy Consumption. *Adv. Mater.* **2018**, *30*, 1800140. [[CrossRef](#)]

38. Ma, X.C.; He, Y.Y.; Zhang, D.X.; Chen, M.J.; Ke, S.C.; Yin, Y.X.; Chang, G.G. Cobalt-Based MOF-Derived CoP/Hierarchical Porous Carbon (HPC) Composites as Robust Catalyst for Efficient Dehydrogenation of Ammonia-Borane. *ChemistrySelect* **2020**, *5*, 2190–2196. [[CrossRef](#)]
39. Wu, H.; Cheng, Y.J.; Wang, B.Y.; Wang, Y.; Wu, M.; Li, W.D.; Liu, B.Z.; Lu, S.Y. Carbon dots-confined CoP-CoO nanoheterostructure with strong interfacial synergy triggered the robust hydrogen evolution from ammonia borane. *J. Energy Chem.* **2021**, *57*, 198–205. [[CrossRef](#)]
40. Asim, M.; Zhang, S.G.; Wang, Y.T.; Maryam, B.; Sajid, M.; Shi, C.X.; Pan, L.; Zhang, X.W.; Zou, J.J. Self-supporting NiCoP for hydrogen generation via hydrolysis of ammonia borane. *Fuel* **2022**, *318*, 123544. [[CrossRef](#)]
41. Chen, Y.F.; Feng, K.; Yuan, G.T.; Kang, Z.H.; Zhong, J. Highly efficient CoNiP nanoboxes on graphene oxide for the hydrolysis of ammonia borane. *Chem. Eng. J.* **2022**, *428*, 131219. [[CrossRef](#)]
42. Pichler, C.M.; Gu, D.; Joshi, H.; Schuth, F. Influence of preparation method and doping of zirconium oxide onto the material characteristics and catalytic activity for the HDO reaction in nickel on zirconium oxide catalysts. *J. Catal.* **2018**, *365*, 367–375. [[CrossRef](#)]
43. Chen, J.F.; Mao, Y.; Wang, H.F.; Hu, P. Theoretical Study of Heteroatom Doping in Tuning the Catalytic Activity of Graphene for Triiodide Reduction. *ACS Catal.* **2016**, *6*, 6804–6813. [[CrossRef](#)]
44. Duan, L.; Wang, P.; Yu, X.C.; Han, X.; Chen, Y.N.; Zhao, P.; Li, D.L.; Yao, R. The synthesis and characterization of Ag-N dual-doped p-type ZnO: Experiment and theory. *Phys. Chem. Chem. Phys.* **2014**, *16*, 4092–4097. [[CrossRef](#)] [[PubMed](#)]
45. Li, H.J.; Yan, Y.F.; Feng, S.; Chen, Y.R.; Li, L.X.; Zhang, L.; Yang, Z.Q. Hydrogen release mechanism and performance of ammonia borane catalyzed by transition metal catalysts Cu-Co/MgO(100). *Energy Res.* **2019**, *43*, 921–930. [[CrossRef](#)]
46. Mu, J.S.; Xu, J.Y.; Zhou, C.M.; Wang, Q.; Wang, X.G.; Liu, Z.Y.; Zhao, X.J.; Yang, E.C. Self-Supported Oxygen and Molybdenum Dual-Doped Cobalt Phosphide Hierarchical Nanomaterials as Superior Bifunctional Electrocatalysts for Overall Water Splitting. *ChemElectroChem* **2021**, *8*, 103–111. [[CrossRef](#)]
47. Figueiredo, J.L.; Pereira, M.F.R.; Freitas, S.S.A.; Órfão, J.J.M. Modification of the surface chemistry of activated carbons. *Carbon* **1999**, *37*, 1379–1389. [[CrossRef](#)]
48. Delley, B. An all-electron numerical method for solving the local density functional for polyatomic molecules. *J. Chem. Phys.* **1990**, *92*, 508–517. [[CrossRef](#)]
49. Halgren, T.A.; Lipscomb, W.N. The synchronous-transit method for determining reaction pathways and locating molecular transition states. *Chem. Phys. Lett.* **1977**, *49*, 225–232. [[CrossRef](#)]
50. Bahamon, D.; Khalil, M.; Belabbes, A.; Alwahedi, Y.; Vega, L.F.; Polychronopoulou, K. A DFT study of the adsorption energy and electronic interactions of the SO₂ molecule on a CoP hydrotreating catalyst. *RSC Adv.* **2021**, *11*, 2947–2957. [[CrossRef](#)]
51. Cao, X.F.; Tan, Y.; Zheng, H.A.; Hu, J.; Chen, X.; Chen, Z. Effect of cobalt phosphide (CoP) vacancies on its hydrogen evolution activity via water splitting: A theoretical study. *Phys. Chem. Chem. Phys.* **2022**, *24*, 4644–4652. [[CrossRef](#)] [[PubMed](#)]
52. Liu, F.H.; Liu, C.; Zhong, X.L. Enhancing Electrocatalysis for Hydrogen Production over CoP Catalyst by Strain: A Density Functional Theory Study. *Chem. Chem. Phys.* **2019**, *21*, 9137. [[CrossRef](#)] [[PubMed](#)]
53. Chen, T.Y.; Ye, B.; Dai, H.J.; Qin, S.; Zhang, Y.Q.; Yang, Q.H. Ni-doped CoP/Co₂P Nanospheres as Highly Efficient and Stable Hydrogen Evolution Catalysts in Acidic and Alkaline Mediums. *J. Solid State Chem.* **2021**, *301*, 122299. [[CrossRef](#)]
54. Li, K.; Ding, H.L.; Zhou, J.J.; Wang, W.W.; Zhang, P.L. Nitrogen and Molybdenum Co-doped CoP Nanohoneycombs on 3D Nitrogen-doped Porous Graphene as Enhanced Electrocatalyst for Oxygen Evolution Reaction. *Int. J. Hydrogen Energy* **2021**, *46*, 35585–35593. [[CrossRef](#)]
55. Anjum, M.A.R.; Okyay, M.S.; Kim, M.; Lee, H.M.; Park, N.; Lee, J.S. Bifunctional Sulfur-doped Cobalt Phosphide Electrocatalyst Outperforms All-noble-metal Electrocatalysts in Alkaline Electrolyzer for Overall Water Splitting. *Nano Energy* **2018**, *53*, 286–295. [[CrossRef](#)]
56. Yang, Y.Y.; Zhu, C.M.; Zhou, Y.; Zhang, Y.; Xie, Y.D.; Lv, L.W.; Chen, W.L.; He, Y.Y.; Hu, Z.G. Design and synthesis Zn doped CoP/Co₂P nanowire arrays for boosting hydrogen generation reaction. *J. Solid State Chem.* **2020**, *285*, 121231. [[CrossRef](#)]
57. Zhang, Y.; Hui, Z.X.; Zhou, H.Y.; Zai, S.F.; Wen, Z.; Li, J.C.; Yang, C.C.; Jiang, Q. Ga Doping Enables Superior Alkaline Hydrogen Evolution Reaction Performances of CoP. *Chem. Eng. J.* **2022**, *429*, 132012. [[CrossRef](#)]
58. Sun, R.; Bai, Y.; Luo, M.; Qu, M.X.; Wang, Z.H.; Sun, W.; Sun, K.N. Enhancing Polysulfide Confinement and Electrochemical Kinetics by Amorphous Cobalt Phosphide for Highly Efficient Lithium-Sulfur Batteries. *ACS Nano* **2020**, *15*, 739–750. [[CrossRef](#)]